High-frequency microwave detection with GaN HEMTs in the subthreshold regime

Gaudencio Paz-Martínez, Ignacio Íñiguez-De-La-Torre, Philippe Artillan, Héctor Sánchez-Martín, Tomás González, Javier Mateos

High-frequency microwave detection with GaN HEMTs in the subthreshold regime

Gaudencio Paz-Martínez[(1)], Ignacio Íñiguez-de-la-Torre[(1)], Philippe Artillan[(2)],
Héctor Sánchez-Martín[(1)], Tomás González[(1)] and Javier Mateos[(1)]
gaupaz@usal.es, indy@usal.es, philippe.artillan@univ-smb.fr,
hectorsanchezmartin@usal.es, tomasg@usal.es, javierm@usal.es
[(1)]Applied Physics Department and NANOLAB USAL, Univ. Salamanca, Salamanca, Spain
[(2)]Univ. Grenoble Alpes, Univ. Savoie Mont Blanc, CNRS, Grenoble INP, IMEP-LAHC, 38000 Grenoble, France

***Abstract*—The behavior of GaN-based transistors as zero-bias detectors is very dependent on the configuration of the bias, the operation temperature and whether the radio-frequency power is fed in the drain or the gate terminal. In drain-injection, the negative current responsivity shows a bell-shape dependence on V_{GS} for all the studied frequency range and temperatures. In the case of the voltage responsivity, depending on the temperature range an increase or decrease of the responsivity is observed in subthreshold conditions. For the gate-injection configuration, the voltage responsivity at low frequency is null only for $V_{GS} > V_{th}$. Surprisingly, in subthreshold conditions, it is very high and positive, contrary to the negative values expected for this configuration. The origin of this unexpected behavior in $V_{GS} < V_{th}$ is that the drain terminal is self-biased at the zero-current operating point. An analytical model is able to explain the mechanism behind the observed dependencies of the experiments.**

I. Introduction

In the last few years, high electron mobility transistors (HEMTs) based on AlGaN/GaN have been investigated for applications such as broadband communications [1], radar components [2] or space applications [3] because of their excellent frequency and power characteristics. In this work, AlGaN/GaN HEMTs are applied as microwave detectors in the mm-wave region over a wide range of temperatures [4], [5]. We focus our attention on their properties as zero-bias detectors, since excess noise is avoided, but the analysis is not simple because four different configurations can be used depending on whether current or voltage are detected (with short- or open-circuit drain terminal, respectively) or whether the RF power is injected into drain or gate terminals, which we will denote as Drain-Injection (DI) and Gate-Injection (GI) configurations, respectively. Moreover, voltage detection in the subthreshold regions shows a complex behavior due to drain self-biasing, which can be very significant when the transistor has a proper pinch-off behavior [5]. Indeed, in the presence of drain leakage current through the buffer (as happens in GaN HEMTs at low T due to the non ionization of the acceptor ions of the buffer), the DI voltage responsivity in sub-threshold conditions becomes almost null, instead of being quite high (as expected for "good" transistors). However, while the subthreshold behavior within the DI configuration was well explained in [5], the GI case is not yet well understood. In fact, some works have shown that the voltage response is suppressed in the subthreshold region due to loading effects or leakage current [6], [7], [10] but a general explanation of the detection mechanism in GI configuration is still lacking. In this contribution, using expressions for the responsivity based on the Taylor series expansion of the I_D-V_{DS} curves [8], [9], we are able to retrieve and explain the experimental results in all the different configurations where the V_{DS} self-biasing plays a key role.

II. Device under test and experimental setups

We focus our study on a AlGaN/GaN HEMT grown on a high resistivity silicon substrate whose details are provided in [5], [11], [12]. A LakeShore CRX-VF cryogenic probe station is used to perform the measurements in a temperature range of 100-400 K. The layout contains co-planar-waveguide (CPW) accesses to contact the terminals with GSG RF probes. A VNA Keysight N5244A has been used as RF power source up to 43.5 GHz. The insertion losses of the cables and tips have been taken into account to actually deliver a constant RF power, P, at the reference plane of the transistor. The microwave signal in a 1 to 43.5 GHz span is injected either into the drain or the gate terminals. In order to bias both the gate and the drain of the transistor, a two-channel SMU B2902A is used. Two different modes for zero-bias detection will be used: zero-current (ZC) with open-circuit drain, and zero-voltage (ZV) with short-circuited drain. The responsivity in ZC conditions is obtained as the ratio $\beta_v = \frac{\Delta V}{P}$ and in ZV is $\beta_i = \frac{\Delta I}{P}$, where ΔV and ΔI are the DC shift caused by the RF excitation recorded always at the drain terminal and averaged during 5 s. Subscripts d or g are added to distinguish between DI and GI (β_{vd}, β_{vg}, β_{id} and β_{ig}).

III. Results and Discussion

The current responsivity with both DI and GI configurations vs. V_{GS} always shows a bell shape with a maximum 0.2-0.3 V above the threshold bias V_{th} of the transistor and goes down to zero in subthreshold conditions regardless of T, Figs. 1(a) and (b). However, while β_{id} is flat at low frequency and then shows a high frequency roll-off (results not shown here), β_{ig} is suppressed at low frequency due to the capacitive gate-drain coupling. The RF power needs to reach the drain in order to produce a non-zero response [8]. It is also remarkable that DI and GI provide responses with opposite sign, see Fig. 1(b). In the case of the ZC voltage responsivity, Figs. 1(c) and (d), for T <200 K, β_{vd} has a bell shape with a positive maximum near V_{th}, while for T >200 K it increases and saturates when entering the subthreshold region. The origin of this behaviour was already explained in [5], and it is due to the p-type

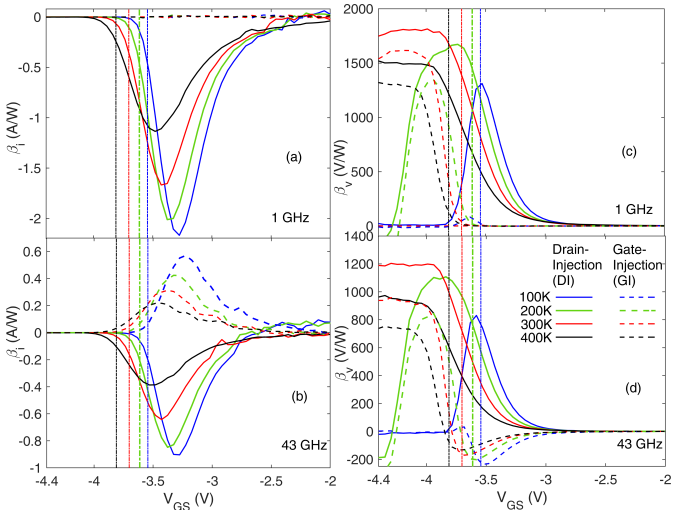

Fig. 1. Zero-voltage (ZV) current responsivity (in A/W) measured at (a) 1 GHz and (b) at 43 GHz and Zero-current (ZC) voltage responsivity (in V/W) at (c) 1 GHz and (d) at 43 GHz as a function of V_{GS} using both Drain-Injection (DI) and Gate-Injection (GI) configurations in the 100-400 K temperature range. The dashed vertical lines indicated the values of V_{th} for each temperature. The experiments were made with a small input RF power of -15 dBm injected to a GaN-HEMT with L_G=250 nm and W=2×25 μm.

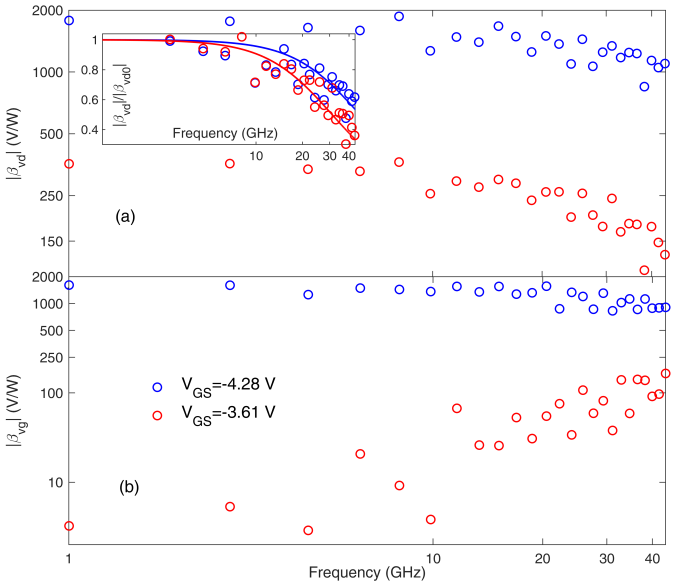

Fig. 2. Zero-current (ZC) responsivity in (a) DI and (b) GI at 300 K for two values of V_{GS}: in subthreshold V_{GS} =-4.28 V $< V_{th}$ and over threshold V_{GS} =-3.61 V $> V_{th}$. The inset shows the normalized β_{vd} measurements (symbols) and fitted data (lines) to a Lorentzian in order to extract the cutoff frequency. Note that both graphs are in plotted in absolute value.

doping of the GaN buffer, which is not active at low T, thus leading to the enhancement of the drain leakage current. In fact, a good transistor pinch off leads to the self-biasing of the drain terminal due to the I_D=0 bias condition, which is only fulfilled for negative V_{DS}, when the transistor enters into the *third-quadrant-conduction* region to generate a non-zero I_D able to compensate the always present gate leakage current. The most significant result of Fig.1 is that obtained for β_{vg}, particularly in the subthreshold region for T >200 K. Surprisingly, β_{vg} is quite large at 1 GHz, while a null value is expected (since at low frequency the gate-drain coupling is negligible). The remarkable sign change of β_{vg} at high frequency when passing from V_{GS} above to below V_{th} is also non expected, since negative values are typically found for β_{vg}.

We can extract more information of these unexpected results by studying the frequency dependence of the ZC voltage responsivity at 300 K. Fig. 2 shows β_{vd} and β_{vg} for two different bias points, one with open channel V_{GS} =-3.61 V $> V_{th}$, and the other corresponding to subthreshold conditions V_{GS} =-4.28 V $< V_{th}$. β_{vd} shows a low-frequency plateau with a high frequency roll-off characterized by a cutoff frequency, f_c. The inset shows the $1/(1+(f/f_c)^2)$ fitting. A value for f_c=47 GHz is found in subthreshold conditions, much higher than that for $V_{GS} > V_{th}$, 31 GHz. On the other hand, in the case of GI, Fig. 2(b), clear differences between the two operation regions are observed:

- In open channel conditions β_{vg} is null at low frequencies until ≈10 GHz where it starts increasing. This high-pass filter behavior is that expected for the GI configuration, since gate-drain coupling is purely capacitive.
- In subthreshold conditions the frequency dependence of β_{vg} resembles that obtained in DI, with similar f_c, so that it cannot be originated by the gate-drain-coupling, and the explanation for this result must be elsewhere.

The analytical model proposed by [9] allows to obtain the voltage responsivity both in DI and GI conditions taking as a base the static coefficients g_{ij} (defined as $g_{ij} = \partial^{(i+j)} I_D / \partial^i V_{GS} \partial^j V_{DS}$) extracted from the I_D-V_{DS} curves using the following equations:

$$\beta_{vd} = -\frac{R_0 R_D}{2}(g_{20}\alpha_d^2 + g_{02} + 2\alpha_d g_{11}\cos\theta), \quad (1)$$

$$\beta_{vg} = -\frac{R_0 R_D}{2}(g_{20} + \alpha_g^2 g_{02} + 2\alpha_g g_{11}\cos\theta), \quad (2)$$

where R_0 is the source output impedance, R_D is the channel resistance, $\alpha_d = v_{gs}/v_{ds}$ and $\alpha_g = v_{ds}/v_{gs}$ are the ratios between the transmitted AC signals to the gate/drain terminals and that input signals, v_{ds} in DI and v_{gs} in GI, respectively, and θ the phase shift between both AC signals.

Fig. 3 shows that for $V_{GS} > V_{th}$, g_{20} is null and g_{02} and g_{11} have opposite signs and similar absolute values with a maximum around V_{GS}=-3.23 V. Remarkably, due to the capacitive gate-drain coupling, at low frequency α_d=α_g=0, so that g_{02} is the only significant parameter for β_{vd} and g_{20} for β_{vg}. The typical assumption is that g_{20} is null because I_D=0, so that the model is able to explain well the low frequency dependence of both responsivities above threshold (and the positive values obtained for β_{vd} and negative for β_{vg}). At high frequency both α_d and α_g increase, and consequently the (negative) contribution of the g_{11} terms, so that the roll-off of β_{vd} and the increase of β_{vg} are also well captured by the model.

However, in subthreshold one would expect to find that $\beta_{vg} = 0$ at low frequency, contrary to what it is obtained in the experiments, Fig. 1(c). The explanation is that g_{20} is not zero in that conditions (see the zoom in the bottom inset of Fig. 3). In fact, it reaches a value similar to g_{02} and with the same sign, so that β_{vd} and β_{vg} take exactly the same values in the subthreshold region. This is possible because for $V_{GS} < V_{th}$

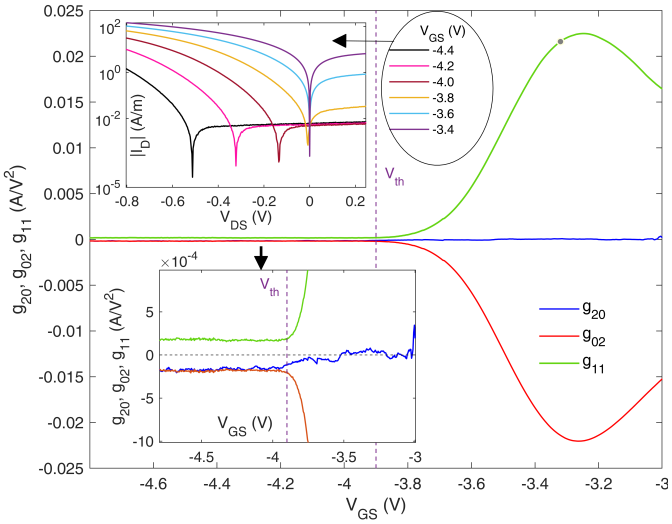

Fig. 3. Taylor series coefficients g_{02}, g_{20} and g_{11} vs. V_{GS} at 300 K. The vertical dotted line indicates the value of V_{th}. The bottom inset corresponds to a zoom around the threshold region. The top inset shows the $|I_D| - V_{DS}$ characteristic of the device.

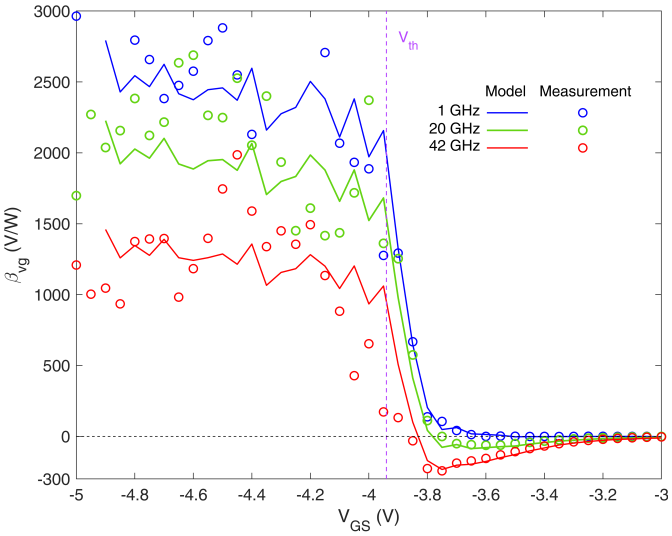

Fig. 4. Comparison of the values of the ZC responsivity β_{vg} *vs,* frequency obtained in the experiments (symbols) and those calculated with equation 2 (solid line) at 300 K for 1, 20 and 42 GHz. The dashed vertical line indicated the value of V_{th}.

the zero I_D point is shifted to negative values of V_{DS} (see the top inset with the $|I_D|$-V_{DS} curves of the transistor in log scale). As a consequence, since the $I_D = 0$ point depends on V_{GS}, the value of $g_{20} = \partial^2 I_D / \partial^2 V_{GS}$ is not null. The very good agreement in the comparison of the experimental values of β_{vg} with those predicted using equation 2 in the whole V_{GS} range for different frequencies is shown in Fig. 4. More information about how this calculation has been performed, mainly concerning the frequency dependence of the $\alpha_d(f)$ and $\alpha_g(f)$ coefficients, will be provided at the conference [13].

IV. Conclusions

We have presented experimental results of zero-bias microwave power detection up to 43 GHz with GaN HEMTs both within the DI and GI configurations in a wide temperature range. While the dependencies on T, V_{GS} and frequency of the detection are well understood for $V_{GS} > V_{th}$ it is not the case in subthreshold conditions, where the drain self-bias plays a key role (mainly for T >200 K). In fact, it allowed us to explain the subthreshold behaviour of β_{vg}. In this contribution we highlight that this mechanism also breaks the usual assumption that g_{20} is null, thus allowing to explain the initially puzzling results, mainly the non-zero values of β_{vg} at low frequency (where the gate-drain coupling is null). With all the terms of equation 2 correctly taken into account, the behavior of the GI voltage responsivity β_{vg} presented in Fig. 1(d) can be well reproduced, Fig. 4, by the model in terms of frequency and V_{GS} dependence.

Acknowledgements

This work has been partially supported through Grant PID2020-115842RB-I00 funded by MCIN/AEI/10.13039/501100011033.

References

[1] J.S. Moon et al., "55% PAE and High Power Ka-Band GaN HEMTs With Linearized Transconductance via n+ GaN Source Contact Ledge," *IEEE Electron Device Lett.,* vol.29 , no. 8, pp. 834-837, Aug. 2008.

[2] K. Kikuchi et al., "An 8.5–10.0 GHz 310 W GaN HEMT for radar applications," *2014 IEEE MTT-S International Microwave Symposium (IMS2014),* pp. 1–4, 2014.

[3] P. Waltereit et al., "GaN HEMTs and MMICs for space applications," *Semiconductor Sci. Technol.,* vol.28 , no. 7, pp. 074010, Feb. 2013.

[4] H. W. Hou, et al., "High Temperature Terahertz Detectors Realized by a GaN High Electron Mobility Transistor," *Jpn. J. Appl. Phys.,* vol.7 , no. 1, pp. 1-6, Ap. 2017.

[5] G. Paz-Martínez, et al, "Temperature and gate-length dependence of subthreshold RF detection in GaN HEMTs," *Sensors,* vol.22 , no. 4, pp. 1515, Feb. 2022.

[6] H. Kojima and T. Asano, "Impact of subthreshold slope on sensitivity of square law detector for high frequency radio wave detection," *Jpn. J. Appl. Phys.,* vol.58 , no. SB, Mar. 2019.

[7] H. Knap, et al., "Nonresonant detection of terahertz radiation in field effect transistors," *J. Appl. Phys.,* vol.99 , no. 11, June 2002.

[8] M. A. Andersson and J. Stake , "An accurate empirical model based on volterra series for FET power detectors," *IEEE Trans. Microw. Theory Techn.,* vol.64 , no. 5, pp. 1431-1441, May 2016.

[9] M. I. W. Khan, S. Kim, D. W. Park, H. J. Kim, S. K. Han, S. G. Lee, "Nonlinear Analysis of Nonresonant THz Response of MOSFET and Implementation of a High-Responsivity Cross-Coupled THz Detector," *IEEE Trans. Terahertz Sci. Technol.,* vol.8 , no. 1, Jan. 2018.

[10] M. Sakowicz, et al., "Terahertz responsivity of field effect transistors versus their static channel conductivity and loading effects," *J. Appl. Phys.,* vol. 110 , no. 5, Sept. 2011.

[11] G. Paz-Martínez, et al., "Comparison of GaN and InGaAs high electron mobility transistors as zero-bias microwave detectors," *J. Appl. Phys.,* vol. 132 , no. 13, Sept. 2022.

[12] G. Paz-Martínez, et al., "Analysis of GaN-based HEMTs operating as RF detectors over a wide temperature range detectors," *IEEE Trans. Microw. Theory Techn.,* to be published, Sept. 2023.

[13] G. Paz-Martínez, et al., "A Closed-Form Expression for the Frequency Dependent Microwave Responsivity of Transistors Based on the I-V Curve and S-Parameters," *Submitted at IEEE Trans. Microw. Theory Techn.*